Johanna Hetterscheidt\*, Lukas Tristl, and Alexander Sutor

# Developing a measurement setup and investigating impact-induced wave propagation in glassfiber-reinforced plastic using acceleration sensors

Entwicklung eines Messaufbaus und Untersuchung der durch Aufschlag induzierten Ausbreitung von Wellen in glasfaserverstärktem Kunststoff mittels Beschleunigungssensoren

https://doi.org/10.1515/teme-2025-0062

Abstract: Mitigating the climate change and preserving biodiversity are both crucial to maintain the Earth's habitability for future generations. While wind energy turbines are urgently needed for sustainable power generation, the threat they pose to already endangered bird and bat species must be addressed. To develop a measurement setup that reliably counts impacts on rotor blades is therefore indispensable to establish effective preventive measures. In this work, we developed a test setup designed to resemble the conditions of a bat or bird strike. Furthermore, we investigated four different sensor types in regard of their feasibility for the intended use case by comparing signal-to-noise ratios, cross-correlations and material related parameters such as wave propagation times and damping factors. The results clearly indicate that two sensors are well suited for further development, and that the proposed setup provides a reliable basis for detailed analysis of the distinct signal characteristics.

**Keywords:** Acceleration sensing; impact detection; ecological measurements

0064-5493

Zusammenfassung: Klimaschutz und der Erhalt der Biodiversität sind entscheidend, um die Lebensbedingungen auf der Erde für zukünftige Generationen zu sichern. Bedrohungen für Tiere, wie gefährdete Vogel- und Fledermausarten durch beispielsweise Windenergieanlagen, müssen dringend reduziert werden. Zur Entwicklung wirksamer Schutzmaßnahmen ist ein Messaufbau zur zuverlässigen Erfassung von Rotorblatt-Kollisionen unverzichtbar. In dieser Arbeit wird ein Testaufbau entwickelt, der die Bedingungen eines Vogeloder Fledermausschlags vereinfacht darstellt. Vier Sensortypen werden auf ihre Eignung anhand von Signal-Rausch-Verhältnissen, Kreuzkorrelationen und wellenphysikalischen Parametern untersucht. Die Ergebnisse zeigen, dass zwei Sensoren gut für die weitere Entwicklung geeignet sind und der Aufbau eine zuverlässige Grundlage für die Analyse der materialspezifischen Signale bietet.

**Schlagwörter:** Beschleunigungsmessung; Aufschlag Detektion; ökologische Messtechnik

# 1 Introduction

The habitats of humans and animals are increasingly threatend by climate change. Rising temperatures resulting from the ongoing emission of greenhouse gases like carbon dioxide cause the surge of extreme weather events such as flooding and periods of extreme heat leading to droughts [1]. Therefore, mitigating the effects of climate change to protect habitats, through a considerable reduction of the greenhouse gas emissions is crucial. Since the combustion of fossil fuels to generate energy is a main contributor to the emission of those gases, one approach to reduce them, is to use renewable energy sources such as wind and solar energy instead [2]. However, wind turbines (WT) are mostly built into grasslands, agricultural land and forests which often overlap with the natural habitats of rare birds and bats.

A not yet precisely known number of animals gets killed or severely injured due to collisions with the moving rotor blades or flying to close which causes barotraumata [3]. Since they are already heavily endangered by modern agriculture and forestry, most bat species are under protection in Europe by the EUROBATS agreement [4] and the EU council directive on the conversation of natural habitats and of wild fauna and flora from 1992 [5]. Even though the precise number of fatalities is not known to date, researchers suspect that the number could be a problem on the population level and therefore lead to the extinction of bat species [6]. This causes a dilemma between the expansion of wind energy plants to mitigate the climate change and the conservation of ecosystems and biodiversity. Therefore, effective measures to prevent collisions must be developed. The main challenge here is to validate these methods, since the current gold standard method to count collisions is to search for carcasses in the surroundings of WT by humans and trained dogs. Unfortunately, the resulting numbers are highly unreliable since no continuous search can be performed and the search area is very big and overgrown in most cases [6, 7]. Consequently, a reliable technical solution to overcome this dilemma is needed. Recent research has investigated using different camera systems (daylight, near-infrared, thermal) to solve this [8], but the following downsides appeared to be non-negligible. They are expensive, sensitive to changing light and weather conditions, hard to implement in bigger scales or offshore settings and often need high computational power. To overcome this, a method to directly detect impacts on the WT rotor blades would be a suitable solution. In our research, we investigate the detection of impacts using acceleration sensors directly mounted to the blades. To provide a suitable solution, extensive knowledge about the involved materials and their impact on the impulse propagation on a blade is needed. In this work we built a simplified setup resembling the involved materials, compared multiple sensors regarding their suitability and investigated the impact induced waves.

## 2 Materials and methods

#### 2.1 Measurement setup

To closely resemble the use case, it is crucial to approximate the material properties of the involved components. The projectiles causing the impacts are bats and birds flying in the surroundings of WT. Biological tissue has very specific material parameters. Since the resulting impulse is highly dependent on the rigidity of the impactor, it is necessary to approximate it by choosing a suitable material. Gelatin is commonly used to mimic biological tissue. However, gelatin is very sensitive and the measurements need to be replicable, so silicone is chosen as a suitable alternative [9]. The silicone mixture used is Smooth-On Ecoflex 00-30 in the ratio 2:1:1. Which is 50 % thinner and 25 % each of component A and B. In our measurement setup the impacts are generated by throwing small silicone spheres and using an impulse hammer with a custom made tip. The custom made tips consist of a 3D-printed base and a silicone hemisphere that was directly cast onto it. The hammer with a mounted tip can be seen in Fig. 1. The sphere weighs 5 g and the radius of it as well as the hemisphere is 21.2 mm. These values are based on the bodies of the smallest bat species native in Europe [10].



Fig. 1: Impulse hammer Sigmatest IH02 with a custom made silicone tip resembling size and material properties of a small bat.

WT rotor blades are made of glass fiber reinforced polymers (GRP) or carbon fiber reinforced polymers (CRP). In industrial production, these materials are laid into a mold in long strips, which is then sealed and filled with epoxy resin. To simplify the material properties and geometry and to avoid anisotropic behaviour, a  $2\,\mathrm{m}\,\times\,1\,\mathrm{m}\,\times$ 0.1 m GRP plate containing randomly oriented glass fibers is used. It consists of 35 % fibers and 65 % epoxy resin. To keep boundary conditions as simple as possible for subsequent research in signal propagation simulation, the plate is mounted horizontally, hanging in an aluminum profile frame using tension straps. To reproduce the impact sites, a grid of width 10 cm spacing in both directions is marked on the plate. The measurement setup is displayed in Fig. 2. The data acquisition setup consists of a Raspberry Pi5B combined with an MCC172 IEPE DAQ HAT by Digilent, which enables the acquiring of analog signals. The sensors used are an integrated electronics piezoelectric (IEPE) microphone (Sigmatest MI21), an IEPE acceleration sensor (Endevco Miniature Isotron accelerometer Model 27AM1), and two

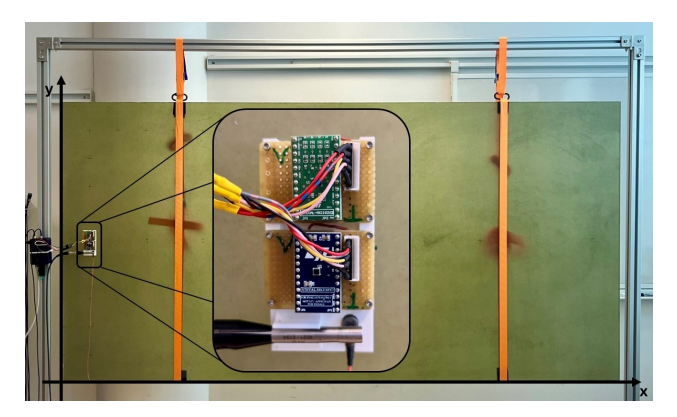


Fig. 2: Measurement setup consisting of hanging GRP plate and the sensor base glued to it in the position  $(10 \, \mathrm{cm}, \, 50 \, \mathrm{cm})$ .

capacitive micro-electro-mechanical systems (MEMS) sensors (STMicroelectronics ISM330DLC and IIS2DH). Both MEMS sensor types consisted of a three-axis accelerometer and the ISM330DLC also contained a three-axis gyroscope. The impulse hammer used is a Sigmatest IH02. The IEPE sensors are connected to the Raspberry Pi via the HAT, while the MEMS sensors are connected directly using an I<sup>2</sup>C interface. The impulse hammer replaces the microphone connected to the HAT. The HAT uses a sampling frequency of 2048 Hz, while the sampling frequency of the MEMS sensors differed between 2000 Hz and 2010 Hz. To ensure minimal and consistent distances between the sensors, they are mounted on a custom, 3D-printed base plate. This plate is glued to the GRP plate using a cyanoacrylate glue (Loctite 401), as suggested by Endevco in [11]. The IEPE acceleration sensor is mounted in a dedicated slot in the base using wax provided by the manufacturer. The sensor patch is positioned at coordinates (10 cm, 50 cm) on the plate as displayed in Fig. 2.

## 2.2 Data acquisition

In order to compare the different sensor types and investigate the wave propagation in the GRP material, two sets of measurements have been performed. In the first set, all four sensors are used simultaneously. A silicon sphere is thrown at the plate, aiming for the coordinates (100 cm, 50 cm), 10 times. This data is then used to calculate the signal-to-noise ratio (SNR) for all sensors and all available axes.

In the second measurement series, the impulse hammer is attached to the DAQ HAT replacing the microphone. Since the microphone detects sound transmitted through air and is therefore prone to disturbances in many environments, it was decided to replace this sensor with the impulse hammer. Acquiring the hammer signal using the HAT ensures the synchronous recording of the impulse force signal and the IEPE acceleration sensor, which is crucial for synchronizing the MEMS sensors during signal processing. In this case, only the acceleration data from the Z-axes of the two MEMS sensors are used since the signals are to be compared and the IEPE sensor only measures this axis. At distances of 20 cm, 60 cm, 100 cm, 140 cm and 180 cm from the sensors, 30 impacts were recorded per location using the hammer. The measurements were conducted in three separate series of 10 impacts each, with a 6s interval between individual impacts. This data is used to compare the sensors using the cross-correlation after the same impact in the time domain. Furthermore, wave propagation speeds, SNR and damping of a single impact are calculated.

## 2.3 Signal processing

All signals are filtered using a 4th order butterworth highpass with a cutoff frequency of  $5\,\mathrm{Hz}$  and a 4th order butterworth lowpass with a cutoff frequency of  $1000\,\mathrm{Hz}$ .

The onset of an impulse is determined using the Z-score and different thresholds suitable for the respective signal. The Z-score indicates how much a data point differs from the mean and is calculated using Eq. 1 where  $s_i$  denotes the respective sample,  $\mu$  is the mean of the signal and  $\sigma$  is the corresponding standard deviation.

$$z_i = \frac{s_i - \mu}{\sigma} \tag{1}$$

A Z-score of 0 indicates that the value coincides with the mean, whereas positive or negative values reflect the number of standard deviations by which the observation deviates above or below the mean, respectively.

In the first data set, individual impulses are extracted using the Z-Scores of the respective signal while in the second data set they are extracted based on the impulse start times calculated using the Z-scores of the impulse hammer signals. A segment from one second before to two seconds after the start of the impulse is extracted and shifted so that the start of the impulse is at time zero in each case. The MEMS signals are resampled to 2048 Hz to allow comparison.

In both sets, the SNR of each segment is calculated for all investigated axes using the signal before the impulse onset as noise reference (n(j)). The SNR is calculated using Eq. 2.

SNR = 
$$10 \cdot \log_{10} \left( \frac{\frac{1}{N} \sum_{i=1}^{N} s(i)^2}{\frac{1}{M} \sum_{j=1}^{M} n(j)^2} \right)$$
 (2)

In the second test, the normalized cross-correlation between all sensors in the time domain is calculated before and after the aforementioned filtering. To compare the temporal alignment and similarity across all sensors at one impact, the normalized cross-correlation  $C(\tau)$  where  $\tilde{s}_1(t)$  and  $\tilde{s}_2(t)$  are the mean-corrected signals as a function of the lag  $\tau$  is computed using Eq. 3.

$$C(\tau) = \frac{1}{\|\tilde{s}_1\| \cdot \|\tilde{s}_2\|} \sum_{t} \tilde{s}_1(t) \cdot \tilde{s}_2(t+\tau)$$
 (3)

Here,  $\tilde{s}_i$  denotes the Euclidean norm of the signal  $s_i$ . The maximum of the absolute value of the cross-correlation function determines the highest similarity and the corresponding lag as shown in Eq. 4

$$(S_{\max}, \tau_{\max}) = \max_{\tau} |C(\tau)| \tag{4}$$

where  $S_{\text{max}}$  is the maximum normalized correlation coefficient and  $\tau_{\text{max}}$  is the associated time lag. This allows for both amplitude and delay comparison between two signals.

To investigate wave propagation speeds, the impulse onset for all sensors is calculated in each segment using the Z-score. The time difference between the impulse's start from the hammer signal and the impulse's start in the sensor signal is then used to calculate an individual propagation speed.

The damping of the impulses is determined by calculating an envelope e(t) of the signal using the Hilbert transform  $(\mathcal{H})$  as shown in Eq. 5

$$e(t) = |s(t) + j\mathcal{H}\{s(t)\}| = \sqrt{s(t)^2 + (\mathcal{H}\{s(t)\})^2},$$
 (5)

and using Eq. 7 to fit the exponential curve f(t) (Eq. 6) to it.

$$f(t) = A_0 e^{-\alpha t} \tag{6}$$

$$(\hat{A}_0, \hat{\alpha}) = \arg\min_{A_0, \alpha} \|e(t) - f(t)\|$$
 (7)

The damping is denoted by the factor  $\hat{\alpha}$ .

# 3 Results

In the first data set, the SNR of all four sensors are compared. The results are displayed in Tab. 1. For the ISM330DLC, it is evident that filtering considerably improves the SNR in all three acceleration axes, while the gyroscope data is very noisy and therefore excluded from further analysis. For the IIS2DH, filtering only slightly improves the SNR. The high noise level is likely due to a discretization error, which is why this sensor is only used in part of the following evaluations. For the 27AM1, it becomes

apparent that the already good SNR is further improved by filtering. The MI21 also shows a slight improvement in SNR, but this sensor is not considered further as it would likely not provide reliable data in a very noisy environment typical of its intended application.

**Tab. 1:** SNR of all axes of all four sensors in dB before and after the filtering.

MEMS Sensors - SNR in dB								
	ISM33	ISM330DLC		IIS2DH				
Axis	Prefil	Fil	Prefil	Fil				
Acx	13.4±3.2	17.4±3.2	-18.7±2.1	2.5±3.1				
Асу	$-28.2 \pm 4.6$	$17.4 \pm 4.4$	$10.7{\pm}2.7$	$10.7 {\pm} 2.7$				
Acz	$3.8 {\pm} 1.8$	$20.4{\pm}2.4$	2.3±2.1	$6{\pm}0.0$				
Gyx	$-12.8 \pm 3.7$	$-12.6 {\pm} 2.4$	-	-				
Gyy	$-14.8{\pm}2.8$	$-7.1 \pm 2.4$	-	-				
Gyz	$-16.8{\pm}1.9$	$-18.7{\pm}2.1$	-	-				
IEPE Sensors - SNR in dB								
	27	MI	MI21					
Axis	Prefil	Fil	Prefil	Fil				
Z	18.8±1.8	24.9±3.4	-	-				
	-	-	10±1.4	$12.1 {\pm} 1.7$				

In the second data set impulses were triggered at varying distances from the sensors using an impulse hammer. The impulse signals were analyzed for the ISM330DLC, IIS2DH and 27AM1 sensors, considering only the acceleration along the z-axis. A signal of an impact at 180 cm is shown in an example in Fig. 3.

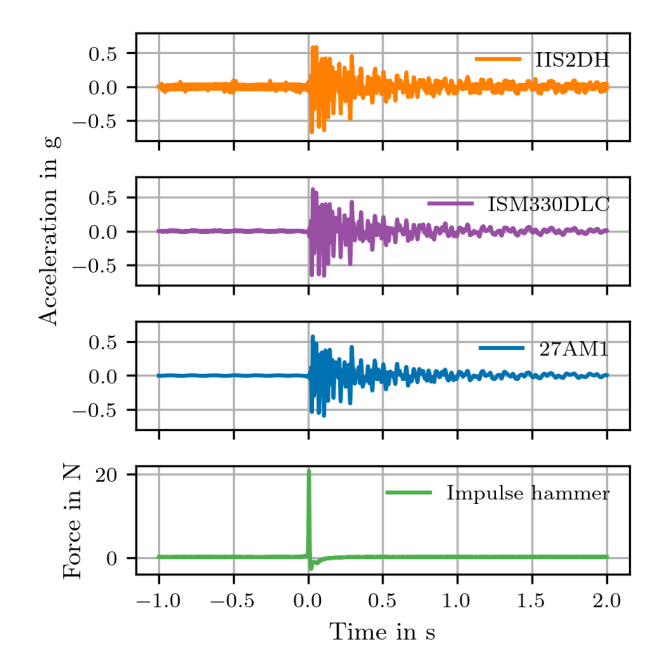


Fig. 3: Time course of the z-axis of an impact measured with all three acceleration sensors at  $180\,\mathrm{cm}$  from the sensors and the corresponding force signal of the impulse hammer.

The SNR results are shown in Tab. 2 and closely match those from data set one. Additionally, it is noticeable that the SNR of the ISM330DLC appears to improve with increasing distance.

**Tab. 2:** SNR of the z-axis of the ISM330DLC, the IIS2DH, and the 27AM1 in dB before and after filtering.

Sensors - SNR in dB								
	ISM330DLC		IIS2DH		21AM1			
Distance	Prefil	Fil	Prefil	Fil	Prefil	Fil		
20 cm	$-1.7\pm1.0$	$2.1\pm~0.3$	$-2.9\pm1.5$	$-1.3\pm1.3$	$18.5\pm2.0$	$26.0\pm2.1$		
60 cm	$\textbf{2.5}\pm\textbf{0.4}$	$6.6\pm1.5$	$1.8\pm0.6$	$\textbf{3.9}\pm\textbf{0.7}$	$22.1\pm1.5$	$30.5\pm2.4$		
100 cm	$\textbf{5.2}\pm\textbf{1.2}$	$14.6\pm1.3$	$4.5\pm1.4$	$\textbf{7.6}\pm\textbf{1.2}$	$21.3\pm1.7$	$29.3\pm3.7$		
140 cm	$5.1\pm2.0$	$18.5\pm1.6$	$4.3\pm2.1$	$\textbf{7.9}\pm\textbf{1.9}$	$21.6\pm2.2$	$40.8\pm3.8$		
180 cm	$6.3\pm1.7$	$\textbf{22.9}\pm\textbf{1.8}$	$\textbf{5.5}\pm\textbf{1.8}$	$\textbf{9.3}\pm\textbf{1.8}$	$21.0\pm1.9$	$\textbf{26.9}\pm\textbf{4.2}$		

Furthermore, the normalized cross-correlation between all three sensors was calculated as shown in Tab. 3. The results show a high degree of correlation between the signals with a very low standard deviation.

**Tab. 3:** Normalized cross-correlation of impulse signals of the *z*-axis between sensors 27AM1, ISM330DLC, and IIS2DH.

Sensors - Normalized cross-correlation								
	27AM1 & ISM330DLC		27AM1 & IIS2DH		ISM330DLC & IIS2DH			
Distance	Prefil	Fil	Prefil	Fil	Prefil	Fil		
20 cm	$0.98 \pm 0.01$	$0.99{\pm}0.00$	$0.85{\pm}0.06$	$0.85{\pm}0.06$	$0.86{\pm}0.06$	$0.86{\pm}0.06$		
60 cm	$0.99 \pm 0.00$	$0.99 \pm 0.00$	$0.91 \pm 0.02$	$0.91 {\pm} 0.02$	$0.92 {\pm} 0.02$	$0.92 {\pm} 0.03$		
100 cm	$0.99 \pm 0.00$	$0.99 \pm 0.00$	$0.91 \pm 0.03$	$0.91 \pm 0.03$	$0.92 {\pm} 0.03$	$0.92 {\pm} 0.03$		
140 cm	$0.99 \pm 0.00$	$0.99 {\pm} 0.00$	$0.90 {\pm} 0.04$	$0.91 {\pm} 0.04$	$0.91 {\pm} 0.04$	$0.91 {\pm} 0.04$		
180 cm	$0.98{\pm}0.00$	$0.99{\pm}0.00$	$0.91{\pm}0.03$	$0.92{\pm}0.03$	$0.93 {\pm} 0.02$	$0.93{\pm}0.02$		

Figure 4 shows the calculated propagation speed of the impact for all distances and for each of the three sensors. The IIS2DH exhibits greater variability than the other sensors. However, it can generally be stated that the medians and means are very close to each other. The 27AM1, in particular, shows relatively low variability. A slight trend can be observed indicating that the propagation speed increases with distance.

Figure 5 shows the mean damping of individual impulses for the 27AM1 and ISM330DLC sensors. It appears that both sensors capture the damping behavior in a very similar manner. Furthermore, the damping appears to decrease with increasing distance from the impact point.

#### 4 Discussion

Both tests demonstrate that the filters applied are appropriate for this application as they lead to notable improvements in the SNRs of the sensor signals. This observation is further supported by the fact that the main part of the signal en-

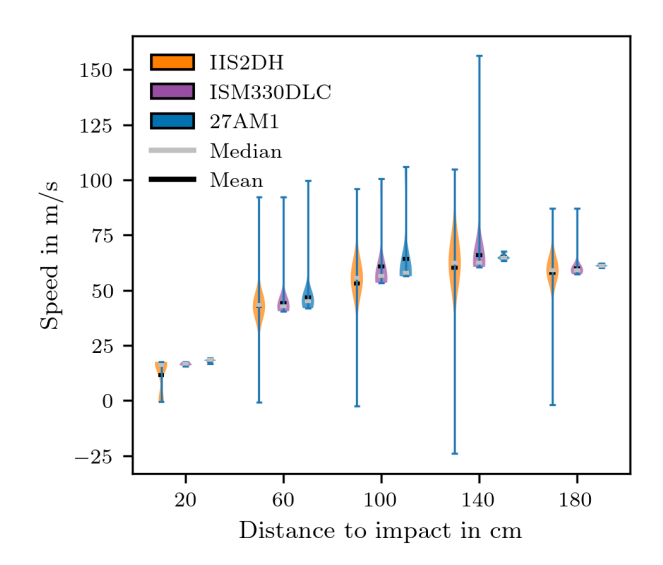


Fig. 4: Wave propagation speed per sensor and per distance for the three sensors 27AM1 (blue), ISM330DLC (green), and IIS2DH (red). Median and mean displayed in gray and black, respectively.

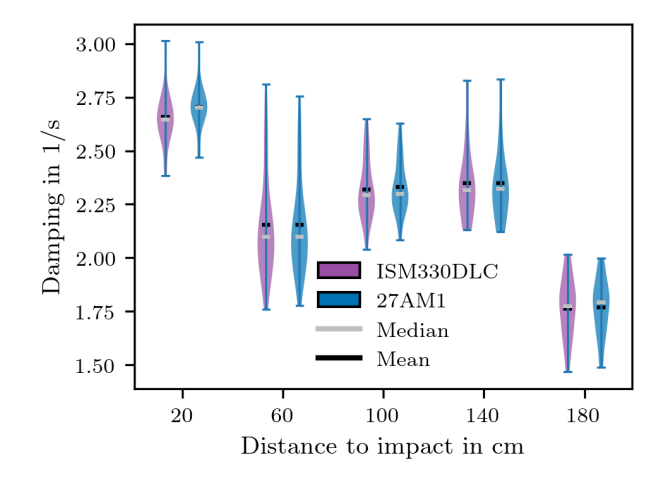


Fig. 5: Wave damping per sensor and per distance for the sensors 27AM1 (blue) and ISM330DLC (green). Median and mean displayed in gray and black, respectively.

ergy in the frequency spectra is concentrated below 250 Hz as previous tests have shown. The low SNRs observed in the gyroscope data are likely due to low angular velocities induced by the applied impacts. In the case of the IIS2DH, the reduced SNR is most likely caused by the previously mentioned discretization error. The MI21 microphone is performing relatively well in the tests. However, there was very little noise disturbances during the data acquisition and it can be expected, that the performance will be considerably worse under real-world operating conditions since there will be higher acoustic levels.

The normalized cross-correlation analysis reveals that the signals are captured highly consistent across all sensors considered, as indicated by the consistently high correlation values and minimal variation over time. It can be concluded, that especially the ISM330DLC MEMS sensor and the 27AM1 piezoelectric sensor perform similarly satisfactory.

The calculated propagation speeds that are shown in Fig. 4 exhibit a relatively large scatter around the mean and median values. In the case of the IIS2DH this is most likely due to the discretization array. Furthermore, the outliers may be due to the fact that the method of detecting the impulse's onset using Z-scores is not always sufficiently reliable. In particular, the first wave is sometimes very small, and the threshold for detecting the impulse onset strongly depends on the impulse strength, making this method difficult to generalize. The observed trend of speed changing with increasing distance suggests that the recorded waves are likely flexural waves. The measured velocity of approximately  $50\,\mathrm{m\,s^{-1}}$  to  $60\,\mathrm{m\,s^{-1}}$  indicates that these could correspond to a mode of Lamb waves [12]. This mode is dispersive, meaning different frequency components propagate at different speeds, causing the signal to distort with increasing distance from the impact location. The differing values in all sensors for the distance of 20 cm could also be attributed to the close proximity between the impact location and the sensors, which prevents the sampling frequency of 2048 Hz from adequately resolving the temporal offset.

The method used to determine the damping produces consistent results. The values shown in Fig. 5 are closely grouped. The slight deviations between the distances may, as with the propagation time, be attributed to the dispersive nature of the impulse. A more detailed analysis of the propagating wave's characteristics and the influence of the material parameters is essential in future investigations.

# 5 Conclusion and outlook

In summary, the results are very promising. The developed test setup can serve as a basis for further development of the measurement system. Regarding the sensors, future research should focus on the ISM330DLC sensor and the 27AM1 IEPE sensor. Additional axes and higher sampling frequencies as well as frequency domain parameters should also be investigated. Furthermore, the wave characteristics and the influence of the GRP material on these should be studied in much greater detail, with particular attention to the wave type and frequency-dependent propagation behavior. To improve propagation time determination, the time delay between signals at different distances could be

analyzed using cross-correlation. A wavelet analysis might also be considered to examine the speeds of different frequency components individually. Subsequently, a simulation of the setup is planned. This could be used to optimize sensor positions and expand the system to larger and more complex geometries. Additionally, the direction-dependent characteristics of the commonly used GRP material could be incorporated.

All of these efforts constitute a promising advancement toward improved protection of bats and birds around WT and thereby facilitate the permitting processes for new installations. Ultimately, this contributes to safeguarding the Earth and preserving its biodiversity for future generations.

# References

- World Meteorological Organization (WMO), State of the Global Climate 2023. Geneva: United Nations, 2024. ISBN: 978-92-63-11347-4.
- [2] United Nations. Paris agreement. 2015.
- [3] Joyce Lee and Feng Zhao. Global Wind Report 2024. Brussels, Belgium: Global Wind Energy Council (GWEC), Apr. 16, 2024.
- [4] UNEP/ EUROBATS, Agreement on the Conservation of Populations of European Bats.
- [5] European Union. Fauna-Flora-Habitat-Richtlinie (FFH-Richtlinie).
- [6] John D. Lloyd et al. "Seasonal patterns of bird and bat collision fatalities at wind turbines". In: PLOS ONE 18.5 (May 2023), pp. 1–17. DOI: 10.1371/journal.pone.0284778.
- [7] A. L. K. Nilsson et al. "Estimating mortality of small passerine birds colliding with wind turbines". In: Scientific Reports 13.1 (Dec. 4, 2023), p. 21365. ISSN: 2045-2322. DOI: 10.1038/s41598-023-46909-z.
- [8] Christof Happ, Alexander Sutor, and Klaus Hochradel. "Methodology for the Automated Visual Detection of Bird and Bat Collision Fatalities at Onshore Wind Turbines". In: *Journal of Imaging* 7.12 (Dec. 9, 2021), p. 272. DOI: 10.3390/jimaging7120272.
- [9] Julia Caldwell and James J. Mooney. "Analysis of Soft Tissue Materials for Simulation Development". In: Simulation in Healthcare: The Journal of the Society for Simulation in Healthcare 14.5 (Oct. 2019), pp. 312–317. ISSN: 1559-713X, 1559-2332. DOI: 10.1097/SIH.000000000000382.
- [10] Christian Dietz. Bats of Britain and Europe. OCLC: 1198442799. Bloomsbury Publishing Plc, 2020. ISBN: 978-1-4729-6318-5.
- [11] Jim Mathews. Guide to Adhesively Mounting Accelerometers. 2022. URL: https://www.endevco.com/contentStore/ mktgContent/endevco/dlm\_uploads/2019/02/TP312.pdf.
- [12] Zhongqing Su, Lin Ye, and Ye Lu. "Guided Lamb waves for identification of damage in composite structures: A review". In: Journal of Sound and Vibration 295.3 (Aug. 2006), pp. 753–780. DOI: 10.1016/j.jsv.2006.01.020.